Benchmarking Coherent Errors in Controlled-Phase Gates due to Spectator Qubits

S. Krinner,[1,*] S. Lazar,[1] A. Remm,[1] C.K. Andersen,[1] N. Lacroix,[1] G.J. Norris,[1] C. Hellings,[1] M. Gabureac,[1] C. Eichler,[1] and A. Wallraff[1,2,†]

[1] *Department of Physics, ETH Zurich, 8093 Zurich, Switzerland*
[2] *Quantum Center, ETH Zurich, 8093 Zurich, Switzerland*

(Received 21 May 2020; accepted 23 July 2020; published 17 August 2020)

A major challenge in operating multiqubit quantum processors is to mitigate multiqubit coherent errors. For superconducting circuits, besides crosstalk originating from imperfect isolation of control lines, dispersive coupling between qubits is a major source of multiqubit coherent errors. We benchmark phase errors in a controlled-phase gate due to dispersive coupling of either of the qubits involved in the gate to one or more spectator qubits. We measure the associated gate infidelity using quantum-process tomography. We point out that, due to coupling of the gate qubits to a noncomputational state during the gate, two-qubit conditional-phase errors are enhanced. Our work is important for understanding limits to the fidelity of two-qubit gates with finite *on-off* ratio in multiqubit settings.

DOI: 10.1103/PhysRevApplied.14.024042

I. INTRODUCTION

In the past two decades the essential building blocks of quantum computers based on superconducting circuits—high-fidelity single-qubit and two-qubit gates, high-fidelity readout, and state initialization—have been developed and steadily improved [1]. An essential requirement for scaling up present quantum processors toward functional universal quantum computers is to ensure that the performance of individual building blocks is maintained when many blocks are combined into a larger processor running operations in parallel. Two-qubit gates are of particular importance since they limit the performance of state-of-the-art quantum processors [1,2]. Although two-qubit-gate errors at the 10^{-3} level have been demonstrated on few-qubit devices or on isolated parts of multiqubit devices [3–7], the gate performance typically degrades when multiple qubits are operated in parallel to perform larger computations [8–13]. Similar observations have been made in quantum processors based on trapped ions [14–17].

For superconducting circuits, two common reasons for this discrepancy are physical crosstalk originating from imperfect isolation of control lines and the difficulty of suppressing unwanted couplings between qubits. The latter contains couplings due to spurious electromagnetic modes as well as couplings present due to finite *on-off* ratios of two-qubit gates. While isolation of control lines and suppression of spurious electromagnetic modes can, in principle, be addressed with careful microwave engineering, finite *off* couplings in the form of dispersive couplings [18–20], also referred to as residual Z-Z couplings, are characteristic of many of the present two-qubit gates [3–6,21–23]. While dispersive coupling is key to quantum nondemolition measurements across many physical platforms [24–29], dispersive coupling in the context of two-qubit gates can lead to coherent errors as well as correlated errors. Both types of errors are known to be particularly harmful in the context of quantum error correction [30–35]. It is therefore important to characterize those errors to their full extent.

Approaches to reduce dispersive couplings include optimizing gate parameters, such as increasing the frequency detuning between qubits in the idle state, applying dynamical decoupling techniques [36–39], designing more-complex passive [40] or tunable [7,10,41–44] qubit-qubit coupling circuits, and combining qubits with opposite anharmonicity [45]. While the dispersive coupling can, in principle, be brought to zero with use of tunable coupling circuits with qubits in a certain frequency-detuning regime, the overhead in terms of circuit complexity and control hardware is significant. This provides motivation to better understand the limitations imposed by dispersive coupling on conventional gate schemes. So far, phase errors due to dispersive coupling have been characterized and mitigated for the constituent qubits in the computational basis [36–39,46–49]. Here we benchmark errors in the two-qubit conditional phase acquired during a controlled-phase gate due to dispersive coupling to up to

*skrinner@phys.ethz.ch
†andreas.wallraff@phys.ethz.ch

three spectator qubits and measure the associated gate infidelity using quantum-process tomography. We show that to understand the conditional-phase error it is necessary to take into account the dispersive shift of the noncomputational state involved in the gate. Our study is conducted with the seven-qubit device introduced in Ref. [50].

II. DISPERSIVE COUPLING BETWEEN GATE QUBITS AND SPECTATOR QUBITS

Two-qubit gates are frequently realized by resonantly coupling computational states with each other or with states outside the computational subspace. One of the most frequently used two-qubit gates is the family of dynamical flux gates, which includes the resonant iSWAP gate [51,52] and the higher-level induced resonant, nonadiabatic [6,53,54] and adiabatic [3,21] controlled-phase gates. In this work we focus on the nonadiabatic controlled-phase gate. Dynamical flux gates rely on the flux tunability of qubit frequencies and are activated by tuning the two-qubit states $|01\rangle$ and $|10\rangle$ into resonance or by tuning the $|11\rangle$ and $|02\rangle$ states into resonance. Here $|0\rangle$, $1\rangle$, and $|2\rangle$ denote the ground state, first excited state, and second excited state of a transmon qubit. In the idling state, when both qubits remain at fixed frequency, the detuning between the two qubits is much larger than the coupling strength between them, ideally fully suppressing the resonant interaction. However, a small dispersive coupling remains. Therefore, any qubit with a physical coupling to the qubits interacting in the gate acts as a spectator qubit, modifying the resonance condition of the gate ($|01\rangle \leftrightarrow |10\rangle$ for the iSWAP gate and $|11\rangle \leftrightarrow |02\rangle$ for the controlled-phase gate) and thereby inducing gate errors.

The dispersive coupling between two transmon qubits, taken here to be a gate qubit G participating in a two-qubit gate and a spectator qubit S, is described by the Hamiltonian

$$H_{\rm disp}/\hbar = (\zeta_1\,|1\rangle_G\langle 1|_G + \zeta_2\,|2\rangle_G\langle 2|_G)\,|1\rangle_S\langle 1|_S; \qquad (1)$$

see Appendix A. The dispersive coupling strengths ζ_1 and ζ_2 are given by

$$\zeta_1 = 2J^2\left(\frac{1}{\Delta+\alpha_S} - \frac{1}{\Delta-\alpha_G}\right),$$
$$\zeta_2 = J^2\left(-\frac{1}{\Delta} + \frac{2}{\Delta-\alpha_G} + \frac{3}{\Delta-2\alpha_G} - \frac{4}{\Delta-\alpha_G+\alpha_S}\right), \qquad (2)$$

where J is the coupling strength, $\Delta = \omega_S - \omega_G$ is the detuning between the qubits, and $\alpha_G = (E_{12,G} - E_{01,G})/\hbar$ [$\alpha_S = (E_{12,S} - E_{01,S})/\hbar$] is the anharmonicity of the gate (spectator) qubit, with E_{ij} denoting the energy difference between the transmon states $|i\rangle$ and $|j\rangle$. The term with prefactor ζ_1 (ζ_2) in Eq. (1) describes the energy shift of the $|1\rangle$ ($|2\rangle$) state of qubit G conditioned on the state of qubit S. For the iSWAP gate, only ζ_1 needs to be taken into account because only computational states are involved in the gate. For the controlled-phase gate we need to take into account both ζ_1 and ζ_2 as discussed in the following paragraphs.

At the heart of the controlled-phase gate is the conditional phase Φ_c acquired by the $|11\rangle$ state. In the presence of a finite detuning $\delta = (E_{|11\rangle} - E_{|02\rangle})/\hbar$ between the $|11\rangle$ state and the $|02\rangle$ state during the gate, Φ_c deviates from its ideal value of π. For the nonadiabatic variant of the gate, which has gate duration $t_g = 2\pi/2\sqrt{2}J$, Φ_c up to first order in δ/J is given by

$$\Phi_c = \pi\left(1 + \frac{\delta}{2\sqrt{2}J}\right). \qquad (3)$$

Hence, a detuning δ arising from dispersive energy shifts of the $|11\rangle$ and $|02\rangle$ states due to coupling to spectator qubits causes a conditional-phase error $\delta\Phi_c = \pi\delta/2\sqrt{2}J$.

We consider the generic case where the two qubits $G1$ and $G2$ interacting in the controlled-phase gate are coupled to a spectator qubit $S1$ and $S2$, respectively; see Fig. 1(a). The energy of the $|11\rangle$ state is shifted by the dispersive interaction with the spectator qubits by an amount $\hbar(\zeta_{1,S1} + \zeta_{1,S2})$, with $\zeta_{1,Si}$ denoting the dispersive shift between the ith spectator qubit Si and its neighboring gate qubit; see Fig. 1(b). The energy of the $|02\rangle$ state is affected only by $S2$ and is dispersively shifted by an amount $\hbar\zeta_{2,S2}$.

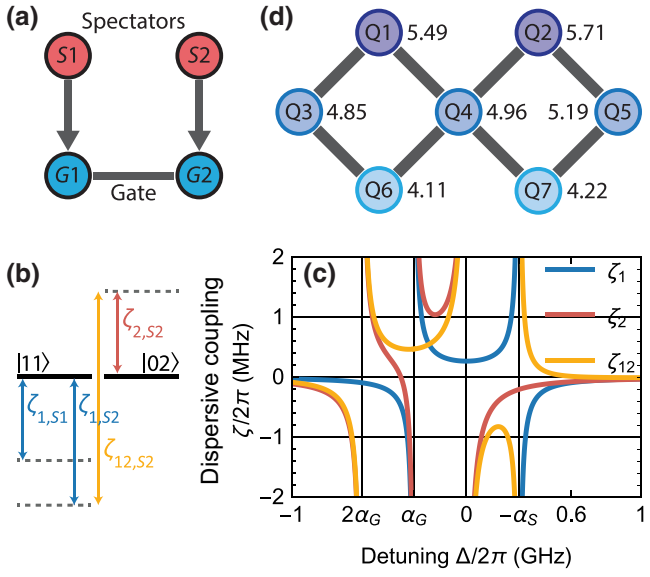

FIG. 1. (a) Spectator qubits $S1$ and $S2$ are coupled to gate qubits $G1$ and $G2$, between which we perform a controlled-phase gate. (b) Energy-level diagram of the states $|G1G2\rangle = |11\rangle$ and $|02\rangle$, which are shifted due to dispersive interaction with the spectator qubits. (c) Dispersive coupling strengths ζ_1, ζ_2, and ζ_{12} as a function of detuning Δ between the gate qubits. (d) Qubit connectivity of the device studied. Numbers next to the qubits indicate qubit idling frequencies in gigahertz.

We thus find a dispersive interaction–induced detuning of

$$\delta = \zeta_{1,S1} + \zeta_{1,S2} - \zeta_{2,S2} = \zeta_{1,S1} - \zeta_{12,S2}, \tag{4}$$

with $\zeta_{12,S2} = \zeta_{2,S2} - \zeta_{1,S2}$ denoting the dispersive shift of the $|1\rangle$-$|2\rangle$-transition frequency conditioned on the spectator qubit being in the $|1\rangle$ state. The dispersive couplings ζ_1, ζ_2, and ζ_{12} are plotted in Fig. 1(c) as a function of detuning Δ for $J/2\pi = 4.5$ MHz and $\alpha_G = \alpha_S = -300$ MHz. While ζ_1 has divergences at the two values $\Delta \in \{\alpha_G, -\alpha_S\}$ due to the Jaynes-Cummings-type couplings $|11\rangle \leftrightarrow |20\rangle$ and $|11\rangle \leftrightarrow |02\rangle$, ζ_2 diverges at the four values $\Delta \in \{2\,\alpha_G, \alpha_G, \alpha_G - \alpha_S, 0\}$ due to the couplings $|21\rangle \leftrightarrow |30\rangle$, $|20\rangle \leftrightarrow |11\rangle$, $|21\rangle \leftrightarrow |12\rangle$, and $|01\rangle \leftrightarrow |10\rangle$, respectively. All aforementioned resonances must be taken into account to understand the limitations imposed on the two-qubit-gate fidelity by spectator qubits.

III. CHARACTERIZATION OF CONDITIONAL-PHASE ERRORS

The connectivity as well as the idling frequencies of the seven qubits Qi on our device [50] are designed for error detection in the surface code; see Fig. 1(d) for a schematic. The idling frequencies are chosen to be the sweet-spot frequencies, at which the qubits are first-order insensitive to flux noise [55]. The coupling strength between neighboring qubits is $J/2\pi \approx 4.5(2)$ MHz. We implement nonadiabatic controlled-phase gates [54] between any pair of neighbors by applying a unipolar, rectangular current pulse to the flux line of one of the qubits. The flux pulse has duration $t_g \simeq 80$ ns and is filtered with Gaussians with $\sigma = 1$ ns. The anharmonicities of the qubits range from -290 to -305 MHz.

We first study the situation in which the spectator qubit acts on the gate qubit that remains in the computational subspace during the gate. For this purpose, we consider Q1 as the spectator qubit and Q4 and Q2 as the gate qubits; see the inset in Fig. 2(c). The detuning between the spectator qubit and the neighboring gate qubit is $\Delta_{Q1,Q4} = 542$ MHz. We first calibrate the controlled-phase gate with the spectator qubit prepared in the $|0\rangle$ state. We measure the conditional phase by performing two Ramsey-type experiments on the gate qubit not neighboring the spectator qubit (here $G2 = $ Q2), with the other gate qubit (here $G1 = $ Q4) prepared in the $|0\rangle$ state and the $|1\rangle$ state, respectively; see Fig. 2(a). In each of theexperiments we vary the angle of the rotation axis of the second $\pi/2$ pulse on the equator of the Bloch sphere by varying the phase of the carrier wave of the pulse, resulting in sinusoidal oscillations of the first excited-state population of Q2; see Fig. 2(b). The phase difference between the two oscillations is the conditional phase Φ_c.

We first calibrate the amplitude and length of the flux pulse such that $\Phi_c = \pi$. We then repeat the conditional-phase measurement with the spectator qubit prepared in the $|1\rangle$ state, and take the difference between the two conditional-phase measurements to obtain the conditional-phase error $\delta\Phi_c$. We average each conditional-phase measurement 3.3×10^4 times and interleave in each repetition the measurements with the spectator qubit in the

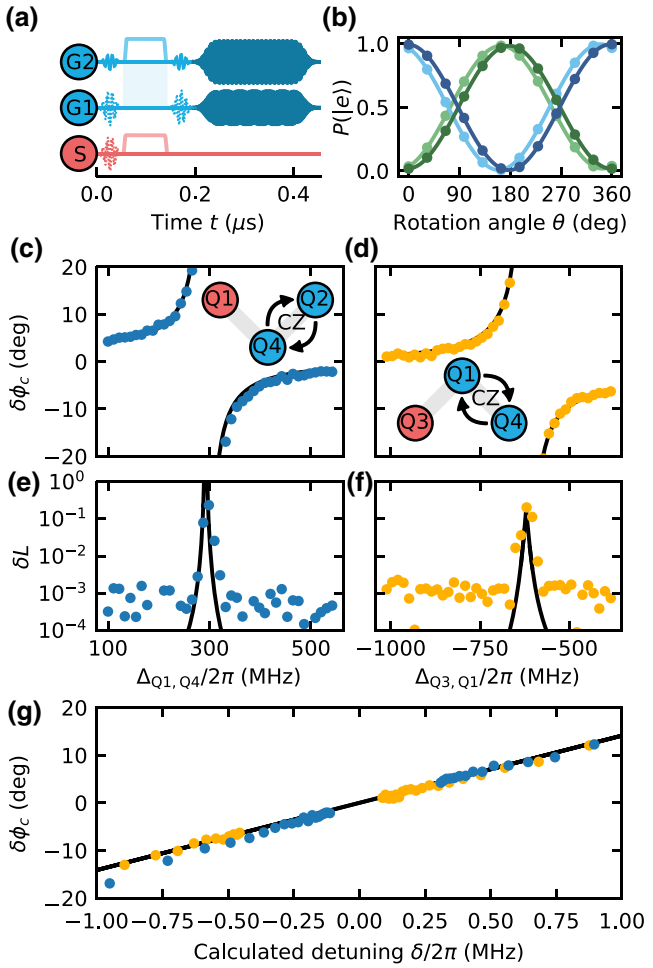

FIG. 2. Conditional-phase and leakage errors due to spectator qubits. (a) Pulse sequence for the conditional-phase measurement. The rectangular pulses are flux pulses, short rf bursts represent $\pi/2$ and π pulses, and long rf bursts at the end represent readout pulses. Dashed pulses indicate that measurements are performed with and without that pulse. (b) Example of a conditional-phase measurement with the spectator qubit in the $|0\rangle$ state (dark-blue and dark-green data) and in the $|1\rangle$ state (light-blue and light-green data). The corresponding sinusoidal fits are shown as solid lines. (c) Conditional-phase error $\delta\Phi_c$ between (c) Q4 and Q2 due to spectator qubit Q1 and between (d) Q1 and Q4 due to spectator qubit Q3 as a function of the detuning between the spectator qubit and its neighboring gate qubit. (e),(f) Corresponding leakage errors. (g) Conditional-phase error $\delta\Phi_c$ from (c),(d) as a function of detuning between the gate qubit states $|11\rangle$ and $|02\rangle$ during the gate. The solid lines in (c),(d),(g) are calculated with Eq. (3) and those on in (e),(f) are calculated with Eq. (5).

$|0\rangle$ and $|1\rangle$ states to reduce noise and the susceptibility to parameter drifts. We obtain $\delta\Phi_c = -2.1^\circ \pm 0.2^\circ$, which is in reasonable agreement with the value calculated with Eq. (3), $\delta\Phi_c = \pi\zeta_1/2\sqrt{2}J = -1.6^\circ$.

Next we study the dependence of the conditional-phase error on the detuning $\Delta_{Q1,Q4}$ between spectator qubit Q1 and gate qubit Q4. For this purpose we vary the frequency of the spectator qubit during the conditional-phase measurement using a flux pulse applied to the flux line of the spectator qubit. We interleave each conditional-phase measurement with a reference measurement in which the spectator qubit is prepared in the $|0\rangle$ state. This is to account for both the spectator state–independent frequency shift of neighboring gate qubit Q4 of $J^2/\Delta_{Q1,Q4}$ and for cross-coupling between the flux line of the spectator qubit and the superconducting-quantum-interference-device loops of the gate qubits. The extracted $\delta\Phi_c$ as a function of $\Delta_{Q1,Q4}$ is shown in Fig. 2(c). We observe that as the detuning is decreased, $\delta\Phi_c$ increases and finally diverges at $\Delta_{Q1,Q4}/2\pi \simeq 289$ MHz, which is the absolute value of the spectator-qubit anharmonicity. The data reflect the dependence of ζ_1 on $\Delta_{Q1,Q4}$ and are well explained by our model $\delta\Phi_c = \pi\zeta_1/2\sqrt{2}J$ (solid line).

We now turn to the situation where the spectator qubit couples to the gate qubit whose $|2\rangle$ state is involved in the gate. Specifically, we choose Q3 as the spectator qubit and Q1 and Q4 as the gate qubits; see the inset in Fig. 2(d). At the idling frequency of the spectator qubit, corresponding to detuning $\Delta_{Q3,Q1}/2\pi = -384$ MHz between the spectator qubit and the neighboring gate qubit, we measure $\delta\Phi_c = -6.3^\circ \pm 0.2^\circ$, in reasonable agreement with the calculated value $\delta\Phi_c = -\pi\zeta_{12}/2\sqrt{2}J = -6.6^\circ$. Analogously to the case described above, we measure the dependence of $\delta\Phi_c$ on $\Delta_{Q3,Q1}$; see Fig. 2(d). $\delta\Phi_c$ increases as we increase $\Delta_{Q3,Q1}$ toward larger negative values, until it diverges and changes sign at $\Delta_{Q3,Q1}/2\pi \simeq -625$ MHz. The data are qualitatively described by our model, which shows a resonance at $\Delta_{Q3,Q1} = 2\alpha_{Q1} + \beta_{Q1}$ due to resonant coupling of the states $|Q1Q3\rangle = |21\rangle, |30\rangle$. Here $\beta_{Q1} = (E_{23} - E_{12})\hbar - (E_{12} - E_{10})/\hbar \approx -35(1)$ MHz is a correction beyond Eq. (2), which takes into account that $E_{23}/\hbar$ differs from $E_{12}/\hbar$ by more than the anharmonicity; see Appendix A.

Since our model for the conditional-phase error, Eq. (3), depends only on the detuning δ between the states $|11\rangle$ and $|02\rangle$ during the gate, it is instructive to plot $\delta\Phi_c$ as a function of δ for both acquired data sets; see Fig. 2(g). Both data sets are well described by the model, showing the expected linear dependence of $\delta\Phi_c$ on δ.

IV. CHARACTERIZATION OF LEAKAGE ERRORS

Besides phase errors, a finite detuning δ during the gate introduces leakage errors (i.e., after the gate a finite fraction δL of the population remains in the $|02\rangle$ state). We determine the leakage error by calculating the time evolution of the gate-qubit populations for gate duration $t_g = 2\pi/2\sqrt{2}J$ using the Hamiltonian $H/\hbar = \sqrt{2}J\,(|0\rangle_{G1}\langle 1|_{G1}|2\rangle_{G2}\langle 1|_{G2} + \text{h.c.}) - \delta|2\rangle_{G2}\langle 2|_{G2}$ describing the resonant gate interaction in the rotating frame. For one of the gate qubits prepared in the $|0\rangle+|1\rangle$ state and the other gate qubit prepared in the $|1\rangle$ state, we obtain in leading order in δ/J

$$\delta L = \frac{1}{2}\left(\frac{\pi}{2}\right)^2\left(\frac{\delta}{2\sqrt{2}J}\right)^4. \tag{5}$$

The leakage error scales with the fourth power of the small parameter δ/J and is therefore significantly smaller than the phase errors.

To determine δL we measure the $|2\rangle$-state population of $|G2\rangle$ at the end of each conditional-phase measurement. Subtraction of the value obtained with the spectator qubit prepared in the $|0\rangle$ state from the value obtained with the spectator qubit in the $|1\rangle$ state yields δL. The extracted values of δL are shown in Figs. 2(e) and 2(f) as a function of the detuning between the spectator qubit and the neighboring gate qubit for the situations corresponding to Figs. 2(c) and 2(d). We observe a sizable leakage error only at detunings corresponding to a divergence of δ, in agreement with a model based on Eq. (5); see the solid lines in Figs. 2(e) and 2(f). The baseline defined by the data corresponds to our measurement accuracy of the $|2\rangle$-state population, which is about 10^{-3}.

V. MULTIPLE SPECTATOR QUBITS

Next we study how errors induced by multiple spectator qubits add up. We consider the controlled-phase gate between Q2 and Q4 and the three spectator qubits Q1, Q6, and Q7 coupling to Q4. The spectator qubits are at their idling frequencies, corresponding to detunings $\Delta_{Q1,Q4} = 542$ MHz, $\Delta_{Q6,Q4} = -844$ MHz, and $\Delta_{Q7,Q4} = -726$ MHz. After calibrating the gate with all spectator qubits in the $|0\rangle$ state, we measure $\delta\Phi_c$ for each of the eight spectator-qubit configurations; see the orange circles in Fig. 3. $\delta\Phi_c$ originating from spectator qubit Q1 isa factor of 3 larger than $\delta\Phi_c$ originating from Q6 and Q7 because the dispersive coupling ζ_1 between Q4 and Q1 is larger than that between Q4 and the other two spectator qubits. For the four configurations with multiple spectator qubits in the $|1\rangle$ state, we observe that the measured $\delta\Phi_c$ agrees well with the sum over the individual contributions, where only a single spectator qubit is in the $|1\rangle$ state. This shows the coherent nature of the spectator qubit–induced conditional-phase errors. Overall our measurements agree well with values calculated with Eq. (3) with independently measured values for ζ_1; see the open squares in Fig. 3.

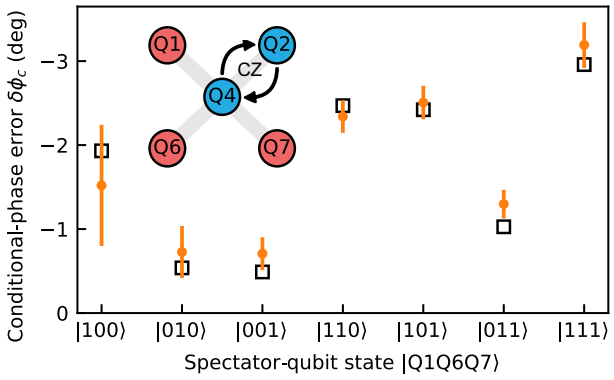

FIG. 3. Measured conditional-phase error $\delta\Phi_c$ (orange circles) in the controlled-phase gate between Q4 and Q2 as a function of spectator-qubit configuration |Q1Q6Q7⟩. Each data point represents the mean of six measurements, and error bars indicate one standard deviation. The open squares are calculated values (see the main text).

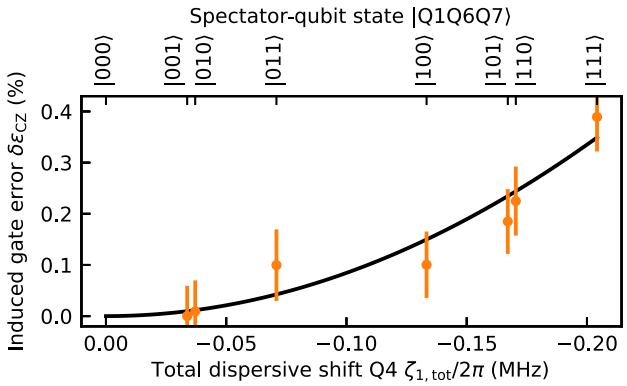

FIG. 4. Increase in controlled-phase-gate error $\delta\varepsilon_{CZ}$ in the presence of multiple spectator qubits as a function of the total dispersive shift of the gate qubit Q4 (orange circles). The top axis indicates the states of the three spectator qubits during each measurement. The solid line is a calculation of the gate error in the presence of phase errors only. Error bars are derived from a bootstrapping method.

VI. PROCESS TOMOGRAPHY

In addition to the conditional-phase error between the gate qubits, the dispersive coupling between a spectator qubit and its neighboring gate qubit also introduces a finite conditional phase between them and therefore mutual dynamical-phase errors, which depend on the state of the distant gate qubit; see Appendix B for details and measurements. Hence, in general, dispersive coupling leads to correlated errors and to an accumulation of entanglement across the system. When we consider the subspace spanned by the gate qubits only, the conditional-phase error between the spectator qubit and the neighboring gate qubit appears as a single-qubit dynamical-phase error $\delta\Phi_d = -\zeta_1(t_g + 2t_b + t_s)$ on the gate qubit, with $t_s =$ 53 ns the duration of a single-qubit gate and $t_b = 5$ ns a buffer time that we add before and after the flux pulse inducing the controlled-phase gate. For the situation corresponding to Fig. 3 we find $\delta\Phi_d \approx -3.5\delta\Phi_c$. However, $\delta\Phi_c$ may exceed $\delta\Phi_d$ in absolute value for spectator qubits coupling to the gate qubit whose $|2\rangle$ state is participating in the gate and for negative $\Delta_{S,G}$; see also Figs. 1(c) and 2(d).

We characterize the joint effect of dynamical-phase and conditional-phase errors on the controlled-phase gate between Q4 and Q2 by extracting the gate errors ε_{CZ} from quantum-process-tomography measurements performed for each of the eight spectator-qubit configurations discussed above. By subtracting the gate error from an interleaved reference measurement with all spectator qubits in the $|0\rangle$ state, we obtain the increase in gate error $\delta\varepsilon_{CZ}$. The reference measurements have a mean gate error ε_{CZ} of 2.7(2)%. To increase the signal-to-noise ratio in our measurement of $\delta\varepsilon_{CZ}$, we perform process tomography of three controlled-phase gates executed in series. To obtain $\delta\varepsilon_{CZ}$ for a single controlled-phase gate, we divide the gate-error increase obtained by 9 because the gate error is a quadratic function of the phase errors; see Appendix C.

We show the extracted values of $\delta\varepsilon_{CZ}$ in Fig. 4 as orange points for each three-spectator-qubit state (top horizontal axis). We find that phase errors are responsible for a gate error of between 0.0% and 0.4% depending on the three-spectator-qubit state. The magnitude of the gate errors introduced by spectator qubits is thus comparable to the magnitude of the gate errors of state-of-the-art implementations of two-qubit gates [3–7].

For the case studied here, both the dynamical-phase error and the conditional-phase error are functions of the total dispersive shift of the gate qubit Q4. The total dispersive shift of Q4 is determined by the spectator-qubit state $|\mathrm{Q1Q6Q7}\rangle = |q_1 q_6 q_7\rangle$, with $q_i \in \{0, 1\}$, and reads $\zeta_{1,\mathrm{tot}} = q_1\zeta_{1,\mathrm{Q1}} + q_6\zeta_{1,\mathrm{Q6}} + q_7\zeta_{1,\mathrm{Q7}}$. We therefore plot $\delta\varepsilon_{CZ}$ as a function of $\zeta_{1,\mathrm{tot}}$; see the bottom horizontal axis in Fig. 4. We compare our data with a calculation (solid line) of the gate error in the presence of coherent phase errors $\delta\Phi_c$ and $\delta\Phi_d$ only; see Appendix C.

We find that the qualitative dependence of $\delta\varepsilon_{CZ}$ on $\zeta_{1,\mathrm{tot}}$ is well captured by this model and shows the quadratic increase expected for coherent phase errors.

VII. CONCLUSION

To conclude, we study how the performance of a controlled-phase gate is affected by the dispersive always-on coupling of the gate qubits to spectator qubits at detunings and coupling strengths typical for our field. We measure conditional-phase errors of up to a few degrees, causing gate errors of up to 0.4%. Our results suggest that

the widely used dynamical flux gate needs further conceptual improvement in order to operate at the 10^{-4}–10^{-3} error level desired for quantum error correction [56,57]. We find that conditional-phase errors are particularly pronounced if the spectator qubit has a lower frequency than the gate qubit whose $|2\rangle$ state is involved in the gate. As a remedy, we propose that in such a configuration, the detuning between the spectator qubit and the gate qubit $|\Delta_{S,G}|$ should be chosen to be significantly larger than $|2\alpha_G|$ for the cases when the spectator qubit is idle and when the spectator qubit is tuned in frequency as part of another gate performed simultaneously. Finally, we envision that dynamical decoupling of idling spectator qubits can be used to mitigate gate errors.

ACKNOWLEDGMENTS

The authors acknowledge contributions to the measurement setup from D. Colao, J. Herrmann, S. Storz, F. Swiadek, and T. Zellweger. The authors acknowledge financial support by the Office of the Director of National Intelligence (ODNI), Intelligence Advanced Research Projects Activity (IARPA), via the U.S. Army Research Office (Grant No. W911NF-16-1-0071), by the National Centre of Competence in Research Quantum Science and Technology, a research instrument of the Swiss National Science Foundation (SNSF), by the EU Flagship on Quantum Technology H2020-FETFLAG-2018-03 project 820363 OpenSuperQ, by SNSF R'equip (Grant No. 206021-170731), and by ETH Zurich. S.K. acknowledges financial support by Fondation Jean-Jacques & Felicia Lopez-Loreta and the ETH Zurich Foundation. The views and conclusions contained herein are those of the authors and should not be interpreted as necessarily representing the official policies or endorsements, either expressed or implied, of the ODNI, IARPA, or U.S. Government.

AUTHOR CONTRIBUTIONS

S.K. conceptualized the work. S.K. and S.L. conducted the experiments. S.L. and S.K. analyzed the data. C.K.A. designed the device, and S.K., A.R., G.J.N., and M.G. fabricated the device. A.R., S.L., C.K.A., N.L., C.H., and S.K. contributed to the experiment-control software. C.E. and A.W. supervised the work. S.K., S.L., and A.W. wrote the manuscript with input from all coauthors.

APPENDIX A: DISPERSIVE HAMILTONIAN

Any pair of coupled transmon qubits on our seven-qubit device, taken here to be a gate qubit G and a spectator qubit S, is described by the Hamiltonian

$$H/\hbar = H_0/\hbar + H_I/\hbar = \sum_{i=G,S}\left(\omega_i \hat{a}_i^\dagger \hat{a}_i + \frac{\alpha_i}{2}\hat{a}_i^\dagger \hat{a}_i^\dagger \hat{a}_i \hat{a}_i\right) + J(\hat{a}_G \hat{a}_S^\dagger + \hat{a}_G^\dagger \hat{a}_S), \tag{A1}$$

where $\hat{a}_G$ and $\hat{a}_S$ ($\hat{a}_G^\dagger$ and $\hat{a}_S^\dagger$) are the lowering (raising) operators of qubits G and S, respectively. We diagonalize the Hamiltonian, expand the eigenenergies to second order in J, and transform the Hamiltonian into the rotating frame with respect to H_0 (i.e., we subtract the unperturbed eigenenergies of H_0 from the diagonal Hamiltonian). The resulting Hamiltonian contains the dispersive interaction terms denoted as H_{disp} in the main text and other dispersive interaction terms not relevant for our study.

To correctly determine the frequency of the resonance of the data shown in Fig. 2(d), we find it necessary to extend the model Hamiltonian H_0, which describes the transmon qubit as an anharmonic oscillator with equally decreasing energy-level separation, $E_{i,i+1} = E_{i-1,i} + \alpha$, by the term

$$\sum_{i=G,S}\frac{\beta_i}{6}\hat{a}_i^\dagger \hat{a}_i^\dagger \hat{a}_i^\dagger \hat{a}_i \hat{a}_i \hat{a}_i. \tag{A2}$$

This term takes into account that the transition frequency from $|2\rangle$ to $|3\rangle$, $E_{23}/\hbar$, differs from $E_{12}/\hbar$ by more than the anharmonicity (i.e., $E_{23}/\hbar = E_{12}/\hbar + \alpha + \beta$). As a consequence, the third term in the equation for ζ_2, Eq. (2), becomes $3/(\Delta + 2\alpha_G + \beta_G)$. We measure $E_{23}/\hbar$ of Q1 by a Ramsey experiment and infer $\beta_{\text{Q1}} = -35(1)$ MHz, in good agreement with the calculated value -31.5 MHz obtained by diagonalization of the transmon Hamiltonian of Q1 [55].

APPENDIX B: DYNAMICAL-PHASE ERRORS

We first present measurements of the single-qubit dynamical-phase errors occurring on Q4 while it performs a gate with Q2. The origin of the error is a dynamical conditional-phase error between Q4 and the spectator qubits Q1, Q6, and Q7, which appears as a single-qubit dynamical-phase error on Q4 when we consider the subspace spanned by the gate qubits Q4 and Q2. For a given spectator-qubit state, the measurement consists of two Ramsey-type experiments on Q4, one with the given spectator-qubit state prepared and one reference experiment with all the spectator qubits prepared in the $|0\rangle$ state. Analogously to the conditional-phase measurement, in each experiment we vary the phase of the second $\pi/2$ pulse and extract the accumulated phase by a sinusoidal fit. The phase difference extracted from the two experiments is the dynamical-phase error $\delta\Phi_d$. The extracted values are

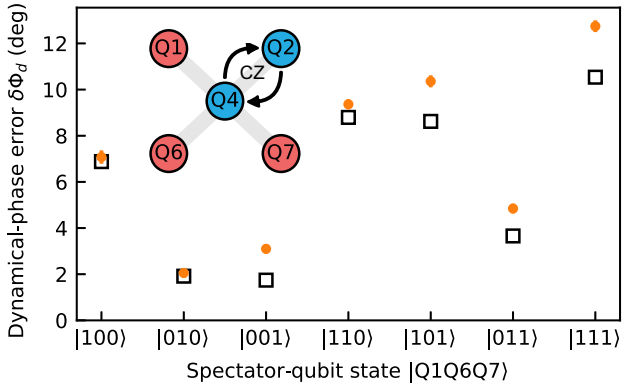

FIG. 5. Dynamical-phase errors in the presence of multiple spectator qubits. Dynamical-phase error $\delta\Phi_d$ (orange circles) on Q4 during the controlled-phase gate between Q4 and Q2 as a function of spectator-qubit configuration |Q1Q6Q7⟩. Each data point represents the mean of two measurements and error bars indicate one standard deviation. The open squares are calculated values (see the text).

shown in Fig. 5 for each spectator-qubit state. The data agree well with values calculated from

$$\delta\Phi_d = -\zeta_{1,\mathrm{tot}}(t_g + 2t_b + t_s); \tag{B1}$$

see the open squares. In our calculation, the values of the dispersive shifts $\zeta_{1,\mathrm{Q1}}/2\pi = -133(2)$ kHz, $\zeta_{1,\mathrm{Q6}}/2\pi = -37(1)$ kHz, and $\zeta_{1,\mathrm{Q7}}/2\pi = -34(1)$ kHz entering $\zeta_{1,\mathrm{tot}}$ are determined from Ramsey experiments.

Since dispersive coupling is mutual, there is also a phase error $\delta\Phi_s$ on the spectator qubits. We measure $\delta\Phi_s$ of Q1 while performing a gate between Q2 and Q4 using a measurement analogous to the one for $\delta\Phi_d$. We obtain $\delta\Phi_s = 7.4(5)^\circ$ [$\delta\Phi_s = 5.8(5)^\circ$] with the distant gate qubit Q2 prepared in the $|0\rangle$ state ($|1\rangle$ state). The dependence of $\delta\Phi_s$ on the state of the distant gate qubit arises due to the state of the neighboring gate qubit Q4 making a round trip between $|1\rangle$ and $|0\rangle$ conditioned on Q2 being in the $|1\rangle$ state. In effect, we expect $\delta\Phi_s = -\zeta_1(t_g + 2t_b + t_s) = 6.9^\circ$ for Q2 prepared in the $|0\rangle$ state and $\delta\Phi_s = -\zeta_1(0.5t_g + 2t_b + t_s) = 5.0^\circ$ for Q2 prepared in the $|1\rangle$ state, in reasonable agreement with our measurements.

Next we measure $\delta\Phi_s$ of Q3 while performing a gate between Q1 and Q4. We obtain $\delta\Phi_s = 13.1(6)^\circ$ [$\delta\Phi_s = 7.6(5)^\circ$] for Q4 prepared in the $|0\rangle$ state ($|1\rangle$ state). Here the dependence of $\delta\Phi_s$ on the state of the distant gate qubit arises due to the state of the neighboring gate qubit Q1 making a round trip between $|1\rangle$ and $|2\rangle$ conditioned on Q4 being in the $|1\rangle$ state. The measured values are in reasonable agreement with the calculated values $\delta\Phi_s = -\zeta_1 t_g - \zeta_{1,\mathrm{id}}(2t_b + t_s) = 12.9^\circ$ and $\delta\Phi_s = -(0.5\zeta_1 + 0.5\zeta_2)t_g - \zeta_{1,\mathrm{id}}(2t_b + t_s) = 6.3^\circ$, respectively. Here $\zeta_{1,\mathrm{id}}$ denotes the dispersive coupling at the detuning corresponding to the idling frequency of Q1.

APPENDIX C: QUANTUM-PROCESS-TOMOGRAPHY GATE ERROR

We calculate the contribution of coherent phase errors to the gate error of a controlled-phase gate. The controlled-phase gate unitary in the presence of a conditional-phase error $\delta\Phi_c$ and single-qubit dynamical-phase errors $\delta\Phi_{d,1}$ and $\delta\Phi_{d,2}$ on gate qubits $G1$ and $G2$ reads

$$U_{\mathrm{CZ}}(\delta\Phi_{d,1}, \delta\Phi_{d,2}, \delta\Phi_c) = \begin{pmatrix} 1 & 0 & 0 & 0 \\ 0 & e^{i\delta\Phi_{d,1}} & 0 & 0 \\ 0 & 0 & e^{i\delta\Phi_{d,2}} & 0 \\ 0 & 0 & 0 & e^{i(\pi+\delta\Phi_c+\delta\Phi_{d,1}+\delta\Phi_{d,2})} \end{pmatrix}. \tag{C1}$$

The gate error or infidelity associated with phase errors $\delta\Phi_c$, $\delta\Phi_{d,1}$, and $\delta\Phi_{d,2}$ only is given by

$$\begin{aligned} \epsilon_{\mathrm{CZ},P} &= 1 - \mathrm{Tr}[\chi_{\mathrm{CZ}}(\delta\Phi_{d,1}, \delta\Phi_{d,2}, \delta\Phi_c), \chi_{\mathrm{CZ}}(0,0,0)] \\ &= 0.75 - 0.125[\cos(\delta\Phi_{d,1}) + \cos(\delta\Phi_{d,2}) \\ &\quad + \cos(\delta\Phi_{d,1} - \delta\Phi_{d,2}) + \cos(\delta\Phi_{d,1} + \delta\Phi_{d,3}) \\ &\quad + \cos(\delta\Phi_{d,2} + \delta\Phi_{d,3}) + \cos(\delta\Phi_{d,1} \\ &\quad + \delta\Phi_{d,2} + \delta\Phi_{d,3})] \\ &\approx 0.25\delta\Phi_{d,1}^2 + 0.25\delta\Phi_{d,2}^2 + 0.1875\delta\Phi_c^2 \\ &\quad + 0.25\delta\Phi_{d,1}\delta\Phi_c + 0.25\delta\Phi_{d,2}\delta\Phi_c, \end{aligned} \tag{C2}$$

where $\chi_{\mathrm{CZ}}(\delta\Phi_{d,1}, \delta\Phi_{d,2}, \delta\Phi_c)$ is the process matrix [58] associated with the two-qubit unitary $U_{\mathrm{CZ}}(\delta\Phi_{d,1}, \delta\Phi_{d,2}, \delta\Phi_c)$. In the last step, we perform a quadratic expansion in $\delta\Phi_{d,1}$, $\delta\Phi_{d,2}$, and $\delta\Phi_c$. We note that the dynamical-phase and conditional-phase errors are each the sum of the individual contributions from each spectator qubit. Furthermore, for the parameter range explored in this study, $\delta\Phi_{d,i}$ and $\delta\Phi_c$ have opposite sign.

For the measurements related to Fig. 4, we have $\delta\Phi_{d,1} = -\zeta_{1,\mathrm{tot}}(t_g + 2t_b + t_s)$, $\delta\Phi_{d,2} = 0$, and $\delta\Phi_c = 0.5\zeta_{1,\mathrm{tot}}t_g$. We find good agreement between our measurements $\delta\epsilon_{\mathrm{CZ}}$ and the calculated values $\epsilon_{\mathrm{CZ},P}$; see Fig. 4.

[1] Morten Kjaergaard, Mollie E. Schwartz, Jochen Braumüller, Philip Krantz, Joel I.-J. Wang, Simon Gustavsson, and William D. Oliver, Superconducting qubits: Current state of play, Annu. Rev. Condens. Matter Phys. **11**, 369 (2020).

[2] Jay M. Gambetta, Jerry M. Chow, and Matthias Steffen, Building logical qubits in a superconducting quantum computing system, npj Quant. Inf. **3**, 2 (2017).

[3] R. Barends *et al.*, Superconducting quantum circuits at the surface code threshold for fault tolerance, Nature **508**, 500 (2014).

[4] Sarah Sheldon, Easwar Magesan, Jerry M. Chow, and Jay M. Gambetta, Procedure for systematically tuning up cross-talk in the cross-resonance gate, Phys. Rev. A **93**, 060302(R) (2016).

[5] M. A. Rol, F. Battistel, F. K. Malinowski, C. C. Bultink, B. M. Tarasinski, R. Vollmer, N. Haider, N. Muthusubramanian, A. Bruno, B. M. Terhal, and L. DiCarlo, Fast, High-Fidelity Conditional-Phase Gate Exploiting Leakage Interference in Weakly Anharmonic Superconducting Qubits, Phys. Rev. Lett. **123**, 120502 (2019).

[6] R. Barends *et al.*, Diabatic Gates for Frequency-Tunable Superconducting Qubits, Phys. Rev. Lett. **123**, 210501 (2019).

[7] B. Foxen *et al.*, Demonstrating a continuous set of two-qubit gates for near-term quantum algorithms, arXiv:2001.08343 (2020).

[8] Jay M. Gambetta, A. D. Córcoles, S. T. Merkel, B. R. Johnson, John A. Smolin, Jerry M. Chow, Colm A. Ryan, Chad Rigetti, S. Poletto, Thomas A. Ohki, Mark B. Ketchen, and M. Steffen, Characterization of Addressability by Simultaneous Randomized Benchmarking, Phys. Rev. Lett. **109**, 240504 (2012).

[9] David C. McKay, Sarah Sheldon, John A. Smolin, Jerry M. Chow, and Jay M. Gambetta, Three-Qubit Randomized Benchmarking, Phys. Rev. Lett. **122**, 200502 (2019).

[10] Frank Arute *et al.*, Quantum supremacy using a programmable superconducting processor, Nature **574**, 505 (2019).

[11] Kenneth Rudinger, Timothy Proctor, Dylan Langharst, Mohan Sarovar, Kevin Young, and Robin Blume-Kohout, Probing Context-Dependent Errors in Quantum Processors, Phys. Rev. X **9**, 021045 (2019).

[12] M. Sarovar, T. Proctor, K. Rudinger, K. Young, E. Nielsen, and R. Blume-Kohout, Detecting crosstalk errors in quantum information processors, arXiv:1908.09855 (2019).

[13] D. C. McKay, A. W. Cross, C. J. Wood, and J. M. Gambetta, Correlated randomized benchmarking, arXiv:2003.02354 (2020).

[14] K. Wright *et al.*, Benchmarking an 11-qubit quantum computer, Nat. Commun. **10**, 5464 (2019).

[15] Alexander Erhard, Joel J. Wallman, Lukas Postler, Michael Meth, Roman Stricker, Esteban A. Martinez, Philipp Schindler, Thomas Monz, Joseph Emerson, and Rainer Blatt, Characterizing large-scale quantum computers via cycle benchmarking, Nat. Commun. **10**, 5347 (2019).

[16] J. P. Gaebler, T. R. Tan, Y. Lin, Y. Wan, R. Bowler, A. C. Keith, S. Glancy, K. Coakley, E. Knill, D. Leibfried *et al.*, High-Fidelity Universal Gate Set for $^{9}Be^{+}$ ion Qubits, Phys. Rev. Lett. **117**, 060505 (2016).

[17] C. J. Ballance, T. P. Harty, N. M. Linke, M. A. Sepiol, and D. M. Lucas, High-Fidelity Quantum Logic Gates Using Trapped-Ion Hyperfine Qubits, Phys. Rev. Lett. **117**, 060504 (2016).

[18] Alexandre Blais, Ren-Shou Huang, Andreas Wallraff, S. M. Girvin, and R. J. Schoelkopf, Cavity quantum electrodynamics for superconducting electrical circuits: An architecture for quantum computation, Phys. Rev. A **69**, 062320 (2004).

[19] A. Wallraff, D. I. Schuster, A. Blais, L. Frunzio, R.-S. Huang, J. Majer, S. Kumar, S. M. Girvin, and R. J. Schoelkopf, Strong coupling of a single photon to a superconducting qubit using circuit quantum electrodynamics, Nature **431**, 162 (2004).

[20] D. I. Schuster, A. A. Houck, J. A. Schreier, A. Wallraff, J. M. Gambetta, A. Blais, L. Frunzio, J. Majer, B. Johnson, M. H. Devoret, S. M. Girvin, and R. J. Schoelkopf, Resolving photon number states in a superconducting circuit, Nature **445**, 515 (2007).

[21] L. DiCarlo, J. M. Chow, J. M. Gambetta, Lev S. Bishop, B. R. Johnson, D. I. Schuster, J. Majer, A. Blais, L. Frunzio, S. M. Girvin, and R. J. Schoelkopf, Demonstration of two-qubit algorithms with a superconducting quantum processor, Nature **460**, 240 (2009).

[22] David C. McKay, Stefan Filipp, Antonio Mezzacapo, Easwar Magesan, Jerry M. Chow, and Jay M. Gambetta, Universal Gate for Fixed-Frequency Qubits via a Tunable bus, Phys. Rev. Appl. **6**, 064007 (2016).

[23] S. A. Caldwell *et al.*, Parametrically Activated Entangling Gates Using Transmon Qubits, Phys. Rev. Appl. **10**, 034050 (2018).

[24] A. Wallraff, D. I. Schuster, A. Blais, L. Frunzio, J. Majer, M. H. Devoret, S. M. Girvin, and R. J. Schoelkopf, Approaching Unit Visibility for Control of a Superconducting Qubit with Dispersive Readout, Phys. Rev. Lett. **95**, 060501 (2005).

[25] J. D. Thompson, B. M. Zwickl, A. M. Jayich, Florian Marquardt, S. M. Girvin, and J. G. E. Harris, Strong dispersive coupling of a high-finesse cavity to a micromechanical membrane, Nature **452**, 72 (2008).

[26] Jakob Meineke, Jean-Philippe Brantut, David Stadler, Torben Müller, Henning Moritz, and Tilman Esslinger, Interferometric measurement of local spin fluctuations in a quantum gas, Nat. Phys. **8**, 454 (2012).

[27] T. Astner, J. Gugler, A. Angerer, S. Wald, S. Putz, N. J. Mauser, M. Trupke, H. Sumiya, S. Onoda, J. Isoya, J. Schmiedmayer, P. Mohn, and J. Majer, Solid-state electron spin lifetime limited by phononic vacuum modes, Nat. Mater. **17**, 313 (2018).

[28] P. Scarlino, D. J. van Woerkom, A. Stockklauser, J. V. Koski, M. C. Collodo, S. Gasparinetti, C. Reichl, W. Wegscheider, T. Ihn, K. Ensslin, and A. Wallraff, All-Microwave Control and Dispersive Readout of Gate-Defined Quantum Dot Qubits in Circuit Quantum Electrodynamics, Phys. Rev. Lett. **122**, 206802 (2019).

[29] Guoji Zheng, Nodar Samkharadze, Marc L. Noordam, Nima Kalhor, Delphine Brousse, Amir Sammak, Giordano Scappucci, and Lieven M. K. Vandersypen, Rapid gate-based spin read-out in silicon using an on-chip resonator, Nat. Nanotechnol. **14**, 742 (2019).

[30] Mauricio Gutiérrez, Conor Smith, Livia Lulushi, Smitha Janardan, and Kenneth R. Brown, Errors and pseudothresholds for incoherent and coherent noise, Phys. Rev. A **94**, 042338 (2016).

[31] Daniel Greenbaum and Zachary Dutton, Modeling coherent errors in quantum error correction, Quant. Sci. Technol. **3**, 015007 (2018).

[32] Sergey Bravyi, Matthias Englbrecht, Robert König, and Nolan Peard, Correcting coherent errors with surface codes, npj Quant. Inf. **4**, 55 (2018).

[33] Stefanie J. Beale, Joel J. Wallman, Mauricio Gutiérrez, Kenneth R. Brown, and Raymond Laflamme, Quantum Error Correction Decoheres Noise, Phys. Rev. Lett. **121**, 190501 (2018).

[34] Paul Baireuther, Thomas E. O'Brien, Brian Tarasinski, and Carlo W. J. Beenakker, Machine-learning-assisted correction of correlated qubit errors in a topological code, Quantum **2**, 48 (2018).

[35] Nishad Maskara, Aleksander Kubica, and Tomas Jochym-O'Connor, Advantages of versatile neural-network decoding for topological codes, Phys. Rev. A **99**, 052351 (2019).

[36] Lorenza Viola and Seth Lloyd, Dynamical suppression of decoherence in two-state quantum systems, Phys. Rev. A **58**, 2733 (1998).

[37] L. M. K. Vandersypen and I. L. Chuang, NMR techniques for quantum control and computation, Rev. Mod. Phys. **76**, 1037 (2004).

[38] J. Bylander, S. Gustavsson, F. Yan, F. Yoshihara, K. Harrabi, G. Fitch, D. G. Cory, Y. Nakamura, J.-S. Tsai, and W. D. Oliver, Noise spectroscopy through dynamical decoupling with a superconducting flux qubit, Nat. Phys. **7**, 565 (2011).

[39] Qiujiang Guo, Shi-Biao Zheng, Jianwen Wang, Chao Song, Pengfei Zhang, Kemin Li, Wuxin Liu, Hui Deng, Keqiang Huang, Dongning Zheng, Xiaobo Zhu, H. Wang, C.-Y. Lu, and Jian-Wei Pan, Dephasing-Insensitive Quantum Information Storage and Processing with Superconducting Qubits, Phys. Rev. Lett. **121**, 130501 (2018).

[40] David C. McKay, Ravi Naik, Philip Reinhold, Lev S. Bishop, and David I. Schuster, High-Contrast Qubit Interactions Using Multimode Cavity QED, Phys. Rev. Lett. **114**, 080501 (2015).

[41] Yu Chen *et al.*, Qubit Architecture with High Coherence and Fast Tunable Coupling, Phys. Rev. Lett. **113**, 220502 (2014).

[42] Fei Yan, Philip Krantz, Youngkyu Sung, Morten Kjaergaard, Daniel L. Campbell, Terry P. Orlando, Simon Gustavsson, and William D. Oliver, Tunable Coupling Scheme for Implementing High-Fidelity Two-Qubit Gates, Phys. Rev. Appl. **10**, 054062 (2018).

[43] Pranav Mundada, Gengyan Zhang, Thomas Hazard, and Andrew Houck, Suppression of Qubit Crosstalk in a Tunable Coupling Superconducting Circuit, Phys. Rev. Appl. **12**, 054023 (2019).

[44] X. Li, T. Cai, H. Yan, Z. Wang, X. Pan, Y. Ma, W. Cai, J. Han, Z. Hua, X. Han, Y. Wu, H. Zhang, H. Wang, Y. Song, L. Duan, and L. Sun, A tunable coupler for suppressing adjacent superconducting qubit coupling, arXiv:1912.10721 (2019).

[45] J. Ku, X. Xu, M. Brink, D. C. McKay, J. B. Hertzberg, M. H. Ansari, and B. L. T. Plourde, Suppression of unwanted *zz* interactions in a hybrid two-qubit system, arXiv:2003.02775 (2020).

[46] L. Steffen, Y. Salathe, M. Oppliger, P. Kurpiers, M. Baur, C. Lang, C. Eichler, G. Puebla-Hellmann, A. Fedorov, and A. Wallraff, Deterministic quantum teleportation with feedforward in a solid state system, Nature **500**, 319 (2013).

[47] Maika Takita, A. D. Córcoles, Easwar Magesan, Baleegh Abdo, Markus Brink, Andrew Cross, Jerry M. Chow, and Jay M. Gambetta, Demonstration of Weight-Four Parity Measurements in the Surface Code Architecture, Phys. Rev. Lett. **117**, 210505 (2016).

[48] Christian Kraglund Andersen, Ants Remm, Stefania Lazar, Sebastian Krinner, Johannes Heinsoo, Jean-Claude Besse, Mihai Gabureac, Andreas Wallraff, and Christopher Eichler, Entanglement stabilization using ancilla-based parity detection and real-time feedback in superconducting circuits, npj Quant. Inf. **5**, 69 (2019), [quant-ph]

[49] C. C. Bultink, T. E. O'Brien, R. Vollmer, N. Muthusubramanian, M. W. Beekman, M. A. Rol, X. Fu, B. Tarasinski, V. Ostroukh, B. Varbanov, A. Bruno, and L. DiCarlo, Protecting quantum entanglement from leakage and qubit errors via repetitive parity measurements, Sci. Adv. **6**, eaay3050 (2020).

[50] Christian Kraglund Andersen, Ants Remm, Stefania Lazar, Sebastian Krinner, Nathan Lacroix, Graham J. Norris, Mihai Gabureac, Christopher Eichler, and Andreas Wallraff, Repeated quantum error detection in a surface code, Nat. Phys. **16**, 875 (2020).

[51] R. C. Bialczak, M. Ansmann, M. Hofheinz, E. Lucero, M. Neeley, A. D. O'Connell, D. Sank, H. Wang, J. Wenner, M. Steffen, A. N. Cleland, and J. M. Martinis, Quantum process tomography of a universal entangling gate implemented with josephson phase qubits, Nat. Phys. **6**, 409 (2010).

[52] A. Dewes, F. R. Ong, V. Schmitt, R. Lauro, N. Boulant, P. Bertet, D. Vion, and D. Esteve, Characterization of a Two-Transmon Processor with Individual Single-Shot Qubit Readout, Phys. Rev. Lett. **108**, 057002 (2012).

[53] Frederick W. Strauch, Philip R. Johnson, Alex J. Dragt, C. J. Lobb, J. R. Anderson, and F. C. Wellstood, Quantum Logic Gates for Coupled Superconducting Phase Qubits, Phys. Rev. Lett. **91**, 167005 (2003).

[54] L. DiCarlo, M. D. Reed, L. Sun, B. R. Johnson, J. M. Chow, J. M. Gambetta, L. Frunzio, S. M. Girvin, M. H. Devoret, and R. J. Schoelkopf, Preparation and measurement of three-qubit entanglement in a superconducting circuit, Nature **467**, 574 (2010).

[55] J. Koch, T. M. Yu, J. Gambetta, A. A. Houck, D. I. Schuster, J. Majer, A. Blais, M. H. Devoret, S. M. Girvin, and R. J. Schoelkopf, Charge-insensitive qubit design derived from the Cooper pair box, Phys. Rev. A **76**, 042319 (2007).

[56] Barbara M. Terhal, Quantum error correction for quantum memories, Rev. Mod. Phys. **87**, 307 (2015).

[57] Markus Reiher, Nathan Wiebe, Krysta M. Svore, Dave Wecker, and Matthias Troyer, Elucidating reaction mechanisms on quantum computers, Proc. Natl. Acad. Sci. **114**, 7555 (2017).

[58] M. A. Nielsen and I. L. Chuang, *Quantum Computation and Quantum Information* (Cambridge University Press, New York, USA, 2011), 10th ed.